PHOTONICS Research

Emerging micro-additive manufacturing technologies enabled by novel optical methods

Wei Lin,[1,2] Dihan Chen,[1] and Shih-Chi Chen[1,*]

[1]Department of Mechanical and Automation Engineering, The Chinese University of Hong Kong, Shatin, Hong Kong, China
[2]Tianjin Key Laboratory of Micro-scale Optical Information Science and Technology, Institute of Modern Optics, Nankai University, Tianjin 300071, China
*Corresponding author: scchen@mae.cuhk.edu.hk

Received 3 August 2020; revised 18 September 2020; accepted 18 September 2020; posted 18 September 2020 (Doc. ID 404334); published 12 November 2020

This paper presents a comprehensive review of recent advances in micro-additive manufacturing enabled by novel optical methods with an emphasis on photopolymerization-based printing processes. Additive manufacturing, also known as three-dimensional (3D) printing, has become an important engineering solution to construct customized components or functional devices at low cost. As a green manufacturing technology, 3D printing has the advantages of high energy efficiency, low material consumption, and high precision. The rapid advancement of 3D printing technology has broadened its applications from laboratory research to industrial manufacturing. Generally, 3D objects to be printed are constructed digitally [e.g., via computer-aided design (CAD) programs] by connecting a 3D dot array, where a dot is defined as a voxel through mechanical, electrical, or optical means. The voxel size ranges from a few orders of magnitude of the wavelength of light to the sub-diffraction limit, achieved by material nonlinearity and precise power thresholding. In recent years, extensive research in optical additive manufacturing has led to various breakthroughs in quality, rate, and reproducibility. In this paper, we review various micro-3D printing techniques, including single-photon and two-photon processes, with a focus on innovative optical methods, e.g., ultrafast beam shaping, digital holography, and temporal focusing. We also review and compare recent technological advances in serial and parallel scanning systems from the perspectives of resolution, rate, and repeatability, where the strengths and weaknesses of different methods are discussed for both fundamental and industrial applications.

https://doi.org/10.1364/PRJ.404334

1. INTRODUCTION

Fabrication of arbitrary and complex 3D objects is one of the core issues of additive manufacturing. In general, three common manufacturing processes are adopted: forming, subtractive, and additive manufacturing. In the forming process, a workpiece is reshaped into the desired geometry. The process does not involve material addition or subtraction, e.g., vacuum molding, superplastic forming, and compression molding [1,2]. As to subtractive manufacturing, it typically requires the use of cutting tools or high-power lasers to remove unwanted parts from the workpiece. Apart from these two approaches, additive manufacturing, i.e., 3D printing, adds, rather than reshapes or removes, materials to construct 3D objects with desired geometry. 3D printing is not only cost effective and energy saving but also delivers results with lower material consumption, better customizability, and higher precision [3–5]. As such, 3D printing has become widely adopted and extensively applied in many fields, e.g., medicine [6–8], microelectronics [9–11], optics [12–15], education [16], and architecture [17]. Moreover, with the introduction of commercial computer-aided design (CAD) software and reasonably-priced printers, design and fabrication of 3D objects are greatly simplified for even untrained people. The once professional manufacturing technique has now become so accessible that it attracts a growing number of users. The global market for 3D printing has been growing at a rate of 20.6% from 2013 to 2020 [18]. The market was valued at $11.58 billion in 2019 and expected at $35.38 billion in 2027 [19].

In 3D printing, an object is constructed and described digitally by a dot array, where a dot, i.e., voxel, represents a minimum printing unit in the same way as it is a pixel in imaging. The voxel size in 3D printing technology ranges from nanoscale to macroscale [5]. Among the different 3D printing technologies, micro-additive manufacturing (or micro-3D printing), which exploits a micrometer or sub-micrometer scale voxel, has been extensively researched due to its capability to fabricate various microproducts, e.g., microelectromechanical systems (MEMS), micro–opto–electro–mechanical systems

(MOEMS), and micro-optical electronics systems (MOES), which are potentially applicable in fields such as sensing, medicine, and communications [20]. As the said fields of science advance, the demand for further miniaturized microproducts is compelling. As opposed to conventional methods, micro-3D printing techniques can effectively facilitate the testing and studying of complex 3D microstructures and elements in small or medium batches. Figure 1 shows the microproducts generated by micro-3D printing technologies [21–26].

In spite of the differences in materials, working mechanisms, or processing methods, micro-3D printing technologies can be categorized as follows: fused filament deposition (FFD) [27–30], direct ink writing (DIW) [31–33], direct energy deposition (DED) [34–37], laminated object manufacturing (LOM) [38,39], electrohydrodynamic redox printing (EHDP) [40,41], powder bed fusion (PBF) [42,43], photopolymerization-based 3D printing (P3DP) [44–48], and laser chemical vapor deposition (LCVD) [49,50]. Table 1 summarizes these approaches in the feedstock material, process, fabrication rate, and resolution [28,29,32–34,36,37,39–41,44–48,50–54]. From Table 1, one may conclude that the optical method (especially P3DP) is one of the most critical processing means due to its strengths in resolution, quality, reproducibility, and rate. First, the resolution in optical 3D printing is determined mainly by the diffraction limit of the illumination system, i.e., $0.61\lambda/\mathrm{NA}$, where λ and NA refer to the wavelength of the light source and numerical aperture of the illumination system, respectively. By using a light source with shorter wavelengths, e.g., UV beam, and an objective with higher NA, a higher resolution can be achieved. The result can be further improved by exploiting material nonlinearity and precise power thresholding [45,53]. (Note that although DED and EHDP achieve higher resolution, the associated high cost and low fabrication rate greatly limit their applications.) Second, the optical method renders a firmer connection of adjacent voxels as opposed to other approaches based on heat treatment and laminating. The post-processing step, such as photo-curing, also contributes to the quality of 3D printing parts [34,51]. Last, the laser spot or optical pattern that processes the feedstock facilitates the stability and reproducibility as a result of the non-contact approach between the processing region and the illumination system.

As many optical 3D printing techniques, including laser-assisted DED, PBF, and LCVD, use a tightly focused laser spot to melt the feedstocks or enhance the chemical vapor deposition, and thereby all share similar optical configurations, comprising a light source, beam collimator, scanning system, and objective. In contrast, P3DP has a diverse system design, as it does not need a tightly focused spot to initiate the photopolymerization process. Many P3DP systems are simultaneously microscopic imaging systems, where the latest microscopy techniques are implemented to enhance the performance. For example, the resolution can be improved by introducing super-resolution microscopy methods, e.g., stimulated emission depletion (STED) [53,55,56]. Therefore, P3DP has been widely investigated as a more appealing optical 3D printing technique. In this review, we will focus on the micro-P3DP technology including single-photon and two-photon processes. We will provide an up-to-date overview for the readers in the optics community and discuss a few selected innovative optical methods for enhancing printing performance in depth. Furthermore, we will review and compare the latest technological advances, e.g., serial versus parallel scanning, in terms of resolution and rate. Finally, we will examine the strengths and weaknesses of different methods for both fundamental and industrial applications.

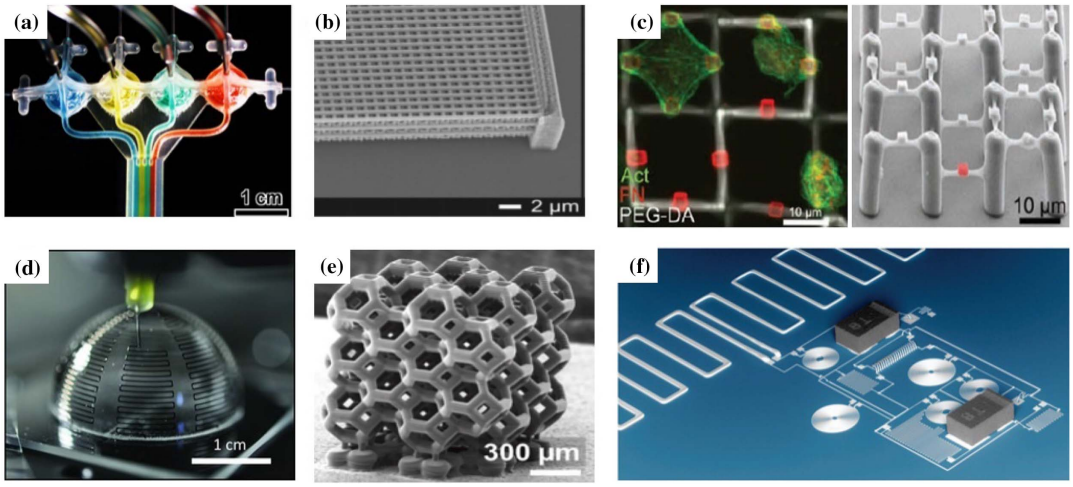

Fig. 1. Microproducts fabricated via micro-3D printing technology: (a) 3D gate pressure-actuated multi-flow controller (reprinted by permission from RSC: Lab on a Chip [21], copyright 2015); (b) photonic crystal (reprinted by permission from Wiley-VCH: Advanced Materials [22], copyright 2006); (c) cell holder (reprinted by permission from Wiley-VCH: Advanced Materials [23], copyright 2011); (d) 3D electrically small antennas (reprinted by permission from Wiley-VCH: Advanced Materials [24], copyright 2011); (e) mechanical metamaterials (reprinted by permission from AAAS: Science [25], copyright 2014); and (f) wireless transmitter clocked by an oscillator (reprinted by permission from Wiley-VCH: Advanced Materials [26], copyright 2017).

Table 1. Summary of Micro-3D Printing Methods in Terms of Material, Process, Fabrication Rate, and Resolution

Approach	Feedstock Material	Process	Printing Rate (mm^3/h)	Resolution (μm)	Potential Applications	References
FFD	Polymer filament	Heat treatment	2×10^3–5×10^3	200–400	Prototyping, advanced composite	[28,29]
DIW	Liquid with dispersion of particles	Coagulation, thermal curing, gluing	2×10^{-3}–4×10^3	0.268–610	Biomedicine	[32,33,51,52]
DED	Metal, alloy	Focused ion/electron beam/arc/laser	7.2×10^{-10}–3.6×10^{-5}	0.008–40	Aerospace, retrofitting, biomedicine	[36,37]
LOM	Polymer, ceramics, metal, alloy, paper	Laminating		30	Electronics, smart structures	[39]
EHDP	Metal, alloy	Application of voltage	7.2×10^{-6}–3.60×10^{-4}	0.07–3	Retrofitting, biomedicine, electronics	[36,40,41]
PBF	Fine powder of polymer, ceramics, metal, alloy	Illumination of focused laser spot	4.5×10^6	80–250	Biomedicine, lightweight structures	[34]
P3DP	Resin (polymer, hybrid polymer-ceramic, functionalized polymer)	Illumination of focused laser spot or optical patterns	6.9×10^{-7}–5.0×10^6	0.052–200	Prototyping, biomedicine	[44–48,53,54]
LCVD	Gaseous reactants	Illumination of focused laser spot	3.15×10^{-1}	40	High purity/quality crystals	[50]

2. PHOTOPOLYMERIZATION

Photopolymerization, a light-induced polymerization process, is a photochemical reaction process that is used to *in situ* form solid structures from liquid photoresin. A series of chemical reactions in the liquid photoresin, typically comprising photoinitiators, monomers, or oligomers and photoinhibitors, is initiated by the energy absorbed from a direct light source and occurs in milliseconds [57]. In other words, when the compound photoresin is illuminated by the radiation source with appropriate wavelength, the initiation procedure, followed by the propagation, immediately starts and ends by the termination and quenching [58,59]. As shown in Fig. 2(a), in the initiation step, photoinitiators, serving as the photoactive substance, are excited electronically and vibrationally from the ground state S_0 to the singlet excited state S_1 by absorbing the energy of one or two photons. While some photoinitiators remain relaxed to the ground state, even being excited by emission fluorescence light, others undergo intersystem crossing (ISC) to a long-living triplet state T_1 and generate primary radicals $R\cdot$ through α-cleavage efficiently [60–65]. As shown in Figs. 2(b) and 2(c), the process is interpreted intuitively. Here, the luminous yellow points represent the dissociative radicals activated by the radiation light source. Subsequently, the active radicals trigger the chain propagation by attacking existing double bonds and producing new single bonds for monomer or oligomer molecules. The chain polymer rapidly increases in weight and changes to a solid state, as shown in Fig. 2(d) [66]. The growth of the polymer chain is stopped in the termination and quenching reaction when a propagating radical or single bond encounters a radical inhibitor (e.g., oxygen) or when two propagating radicals or single bonds encounter one another by side reaction [58,60–62]. The photopolymerized volume, as highlighted by light yellow in Fig. 2(e), is strictly constrained as a result of light exposure to the designed area.

The reaction mechanism for photopolymerization indicates that optical factors including wavelength, power density, and exposed volume are critical to the final polymerization results in resolution, solidification rate, and surface roughness. For single-photon polymerization, either a laser source or light emitting diode (LED) with visible wavelength satisfies the required power threshold, with the axial resolution largely compromised by the accumulation effect [67,68]. With a femtosecond ultrashort pulse laser, two-photon polymerization can reach an ultimate high resolution along both lateral and axial directions due to a nonlinear absorption cross section [69,70]. The cost of nanofabrication is presumably higher, but the increase in cost can be justified by the improved resolution and capability. The polymerization result is also affected by the type and concentration of the photoinitator and photoinhibitor used in the optical system given its different reaction efficiency and diffusion velocity [71]. In recent years, photoresins have been extensively

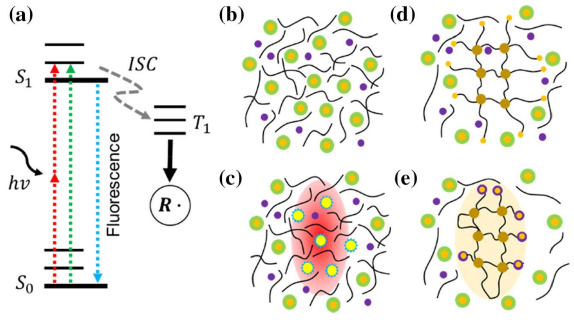

Fig. 2. (a) Energy-level diagram for photoinitiator molecules for one-photon and two-photon excitation. $h\nu$, photon energy; S_0, ground state; S_1, excited singlet state; T_1, triplet state; ISC, intersystem crossing. (b)–(e) Schematic of the reaction mechanism for liquid photoresin containing monomers/oligomers (black lines), photoinitiators (green annulus) with radicals (yellow circles), and photoinhibitors (purple dots) (b) before and (c) after initiation, where the red area is illuminated by the irradiation source, and the blue corona is the emission fluorescence. Schematic of the sequential reaction mechanism for (d) chain reaction propagation and (e) termination/quenching procedure. The shaded yellow area represents the photopolymerized volume.

researched in terms of printing resolution, rate, and materials, leading to direct printing of functional devices [72]. For example, new water-soluble and visible-light photoinitiators pave the way for printing low-cost biomaterials. New monomers, oligomers, and functional materials enable the engineering and optimization of printed objects in terms of, for example, toughness, flexibility, and shape memory characteristics [72–75].

3. OPTICAL METHODS FOR 3D PRINTING—FROM SERIAL SCANNING TO VOLUMETRIC MANUFACTURING

Photopolymerization enables 3D printing by connecting voxels via different optical methods. These methods, each demanding a different optical system, are classified into point-scanning, layer-scanning, and volumetric manufacturing, depending on the dimension of printing elements for single exposure, i.e., point, plane, or volume. In recent years, innovative optical methods have been developed to improve the 3D printing performance. In this section, we will review these three optical micro-3D printing methods and their fundamental principles, with an emphasis on comparing their respective precision and speed.

A. Point-Scanning-Based Fabrication

In the point-scanning method, also known as direct laser writing, a single voxel or multiple discrete voxels are generated with one exposure to serially construct a 3D object for printing. The single-photon point-scanning manufacturing technique was proposed in the early 1990s [76], where the lateral resolution is diffraction limited and governed by the NA of the objective. The introduction of ultrafast lasers has rapidly replaced one-photon-based techniques with two-photon-based point-scanning manufacturing techniques, as the axial resolution is substantially improved [44]. When the objective of the illumination system is fixed, the 3D printing performance, especially the throughput, is determined mainly by the scanning method. Figure 3 shows the main scanning setups for point-scanning 3D printing systems. Figures 3(a) and 3(b) present systems that print with a single focus and, respectively, use a 3D translational stage and beam deflecting unit [77]. In Fig. 3(a), the light is focused into the photoresin to generate a voxel. By moving the XYZ stage, a 3D object is fabricated. When the light is scanned to an undesired region, it can be blocked by using a shutter or an intensity modulation device [44,45,78]. The manufacturing volume is determined by the travel range of the stage in three dimensions, which allows large parts (e.g., centimeter scale) to be printed. However, the throughput is rather low due to the limited speeds of translational stages. In Fig. 3(b), an optical deflector is employed to change the incident angle of the collimated beam so that the position of the focus spot changes in the writing plane, which accordingly defines a 2D pattern. Galvo-scanners are a typical component for lateral scanning [79]. Last, 3D printing is achieved by axial scanning via a translational stage [79], piezoelectric objective scanner [80], etc. Due to the low inertia of the optical deflectors, the throughput is much higher than that of the XYZ-stage-based method. Despite its work volume being limited by the field of view (FOV) of the objective, this scanning method is still appealing to meet the demand for high-resolution micro-3D printing and thus is extensively adopted in many commercial systems.

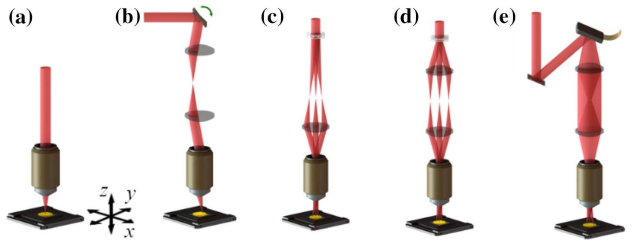

Fig. 3. Main scanning methods for point-scanning 3D printing based on (a) XYZ translational stage and (b) optical deflection via beam delivery components. Main methods to generate multiple foci for 3D printing based on (c) microlens array; (d) diffractive optical elements (DOEs); and (e) spatial light modulator (SLM).

The research focus of 3D printing has been on improving the throughput, and currently, the throughput of point-scanning methods ranges from 10 s to 10^6 voxels/s for single-focus systems [79,81]. One known method is through increasing the number of the laser foci (N), in resist. Several optical elements have been introduced to generate multiple foci, such as aperture arrays, microlens arrays, diffractive optical elements (DOEs), and spatial light modulators (SLMs), as shown in Figs. 3(c)–3(e) [82–86]. The pioneering work on multi-focus 3D printing was proposed by Satoshi Kawata's group in 2005 [87], where the group employed a micro-lens array containing a 41 × 41 lens with a spacing of 250 μm to achieve a throughput of 21 voxels/s. A total of 227 structures were fabricated in parallel with good intensity uniformity. The lateral and axial scanning was achieved, respectively, by 2D stepping motions of the micro-lens array with a resolution of ∼100 nm. While the micro-lens array generated hundreds of foci, such a system disallowed the use of galvo-scanners for lateral scanning due to the astigmatism inevitably induced by large-angle beam incidence. In order to use galvo-scanners, the number of foci needs to be reduced to avert potential aberration. In another design, multi-focus high-speed parallel 3D printing based on galvo-scanners and SLMs has been proposed [88,89]. Initially, the throughput is improved by a factor of N in comparison with the single-focus technique. Nevertheless, the improvement is lower than N times because the split laser beam has reduced power in each focus below the required level for rapid scanning. As to the two-photon system, which requires more optical components, the two-photon absorption efficiency is inevitably reduced due to dispersion and broadened laser pulse. The setback, however, can be compensated for by choosing the appropriate foci number, increasing incident laser power, and inserting group-velocity dispersion compensation elements.

Recently, Hahn *et al.* proposed a rapid multi-focus two-photon printing technique with a throughput up to 10^7 voxels/s [90]. Figure 4(a) shows the schematic for the technique. The group adopted several significant means to achieve such high throughput. First, instead of a shutter, they employed an acoustic optical modulator (AOM) for rapid beam power control with a speed up to 1 MHz. Second, they used a

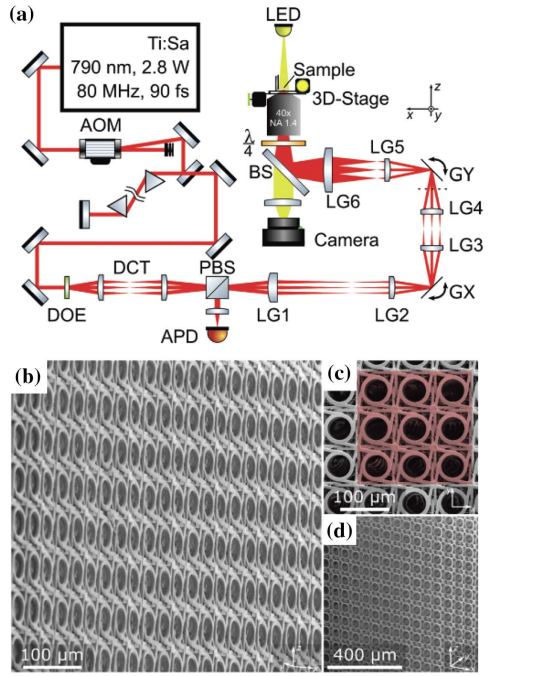

Fig. 4. Rapid multi-focus two-photon printing technique: (a) schematic for the 3D printing system and (b)–(d) scanning electron micrographs of the 3D printed mechanical metamaterial (reprinted from Wiley-VCH: Advanced Functional Materials [90], copyright 2020).

DOE to generate a proper number of foci, i.e., 3 × 3, to ensure the power of each focus was sufficient for the galvo-scanner. A pair of prisms and a dispersion compensating telescope were used to compensate for the dispersion introduced by the optical components, especially the AOM and DOE, to ensure two-photon absorption efficiency. As such, a scanning speed of 0.4 m/s was able to be applied to the galvo-scanning system to achieve high throughput. As shown in Figs. 4(b)–4(d), chiral [Fig. 4(b)] and achiral [Fig. 4(d)] 3D printed mechanical metamaterials are demonstrated with 108,000 3D unit cells, where the printed 3 × 3 array is marked in red [Fig. 4(c)]. The sample containing 3×10^{11} voxels was printed at a speed of 9×10^{7} voxels/s, which is 100 times faster than the previously reported single-focus two-photon system [79,91]. This technique is a potentially powerful tool in the field of metamaterials.

Nonetheless, a multi-focus scanning 3D printing technique based on DOE is restricted to the fabrication of periodic structures. Also, with the galvo-scanner, the point-by-point scanning continues until the entire working space is covered, and a shutter or AOM is also required to switch on/off of the laser to avert the unwanted voxels [92,93]. In other words, a large amount of the scanning points are redundant, hence compromising the manufacturing efficiency. To solve this problem, the holographic multi-focus 3D printing technique is introduced to generate multiple foci that can be randomly accessed. The foci can be controlled individually, and the scanning covers only the desired dots. This technique allows for the fabrication of complicated aperiodic 3D structures with high efficiency. In 2014, Vizsnyiczai *et al.* proposed a holographic multi-focus 3D two-photon printing method based on real-time calculated holograms [94], where five laser foci were used to generate different 3D microstructures in parallel. The positions of the foci were controlled by the holograms displayed on the SLM. As such, the foci scanned only the desired position, thereby improving the scanning efficiency. It should be noted that the scanning speed is limited by the switch of the hologram, i.e., the refresh rate of the SLM.

A feasible method to improve the throughput of holographic 3D printing is by increasing the number of foci. Recently, Manousidaki *et al.* proposed a 3D holographic focal volume engineering method for two-photon 3D printing [95]. In this method, a large number of foci were generated with small spacing as per the designed geometry to reduce the required holograms. The group proposed a phase engineering method to avoid interference between the adjacent foci. Figures 5(a)–5(c) illustrate the optical schematic for the proposed 3D printing system. By switching the holograms displayed on the SLM, the discrete foci bundle, once generated, moves with micro-displacements serially. Figure 5(d) shows the printed chiral structures with 20 foci. The three-layer structure (left) was completed using 51 holograms in approximately 19 s. The six-layer structures (right) were completed using 102 sequential phase masks in 38 s. In contrast with traditional single-focus scanning 3D printing methods, this method enables the fabrication of complete 3D arbitrary structures with 20 times the throughput.

An effective method to further improve the throughput of holographic 3D printing is to employ a high-speed spatial light projection device. With a pattern refresh rate up to 22.7 kHz, a digital micromirror device (DMD) is well suited for fast light projection and has been extensively used in the development of

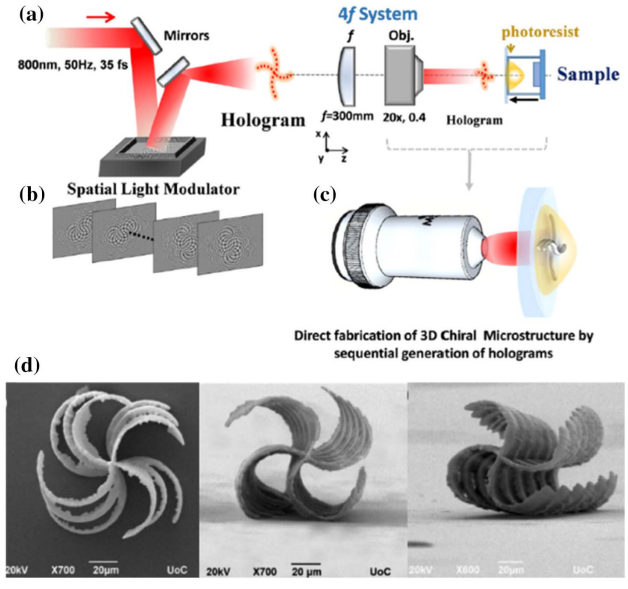

Fig. 5. Holographic multi-focus 3D printing technique: (a) system schematic; (b) serial hologram in the printing process; (c) 4–f system for adjusting the size of the printed parts; and (d) 3D objects printed by the system (reprinted by permission from OSA: Optics Letters [95], copyright 2019).

biosensors, microscopy, and laser fabrication systems [96–100]. In recent years, DMD's strength in high throughput has been substantiated in the context of high-speed random-access scanning [101–103]. In 2019, our group proposed an ultrafast multi-focus 3D nanofabrication method based on binary holography and DMD [104]. Figure 6(a) shows the schematic of the DMD-based multi-focus 3D printing system, where a grating is used to pre-compensate for the angular dispersion introduced by the DMD. Multiple foci are generated by the binary holograms displayed on the DMD. The number of foci and their positions in the working space can be easily controlled by the holograms. Figure 6(b) shows the model and scanning electron microscope (SEM) view of the printing results of the octet truss by using a single focus via the system, where the ~60,000 points in the structure necessitate an equal amount of holograms. The fabrication time is about 30 s at a refresh rate of 2 kHz, or 2.64 s at 22.7 kHz. Figure 6(c) shows the woodpile structure fabricated by the proposed system with a single focus, two foci, and three foci. The total number of the required hologram is reduced by a factor of the number of foci to 21,600, 10,800, and 7200, respectively. Meanwhile, the fabrication time is reduced from 10.8 s to 3.6 s at a refresh rate of 2 kHz. The DMD-based multi-focus random-access 3D printing technique accomplishes large-scale nano-prototyping and the creation of complex structures, overcoming the many challenges associated with conventional raster-scanning-based systems, e.g., printing of complex overhanging structures without supporting materials. Notably, compared to mechanical scanning, the digital scanning methods present better structure reproducibility.

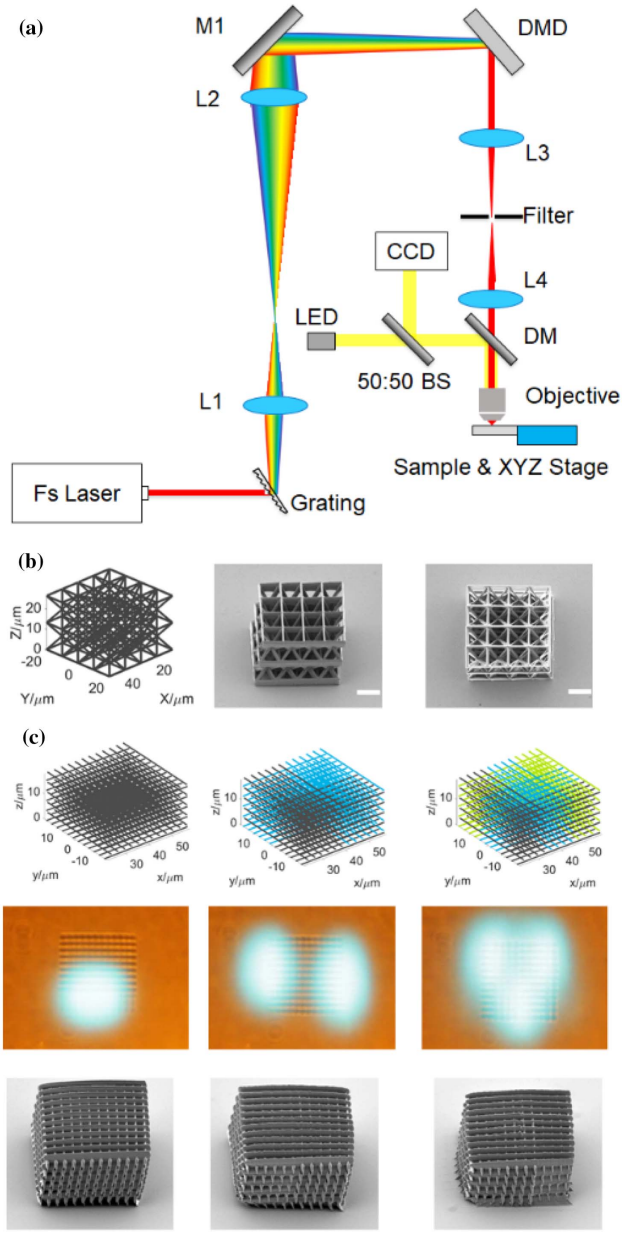

Fig. 6. DMD-based multi-focus 3D printing technique: (a) schematic for DMD 3D printing system; (b) model and SEM images of printed results of octet truss realized by single-focus two-photon polymerization; and (c) comparison of fabrication results of woodpile structures with single focus, two foci, and three foci (reprinted from Springer Nature: Nature Communications [104], copyright 2019).

It should be noted that regardless of the progress, the throughput of the 3D printing techniques is still constrained. With the increase in size of the target 3D structure, the fabrication time also increases significantly. To further improve the throughput of the 3D printing technology, researchers steer their focus towards layer-scanning-based fabrication processes that define an entire layer of a 3D structure at a time in parallel.

B. Layer-Scanning-Based Fabrication

Layer-scanning-based 3D printing, also known as projection microstereolithography (PμSL), is developed from an optical lithography technique. In this method, the 3D slices, decomposed from a 3D object, are serially fabricated in a layer-by-layer fashion axially. This method, first proposed by Bertsch *et al.* in 1997 [105], employs a liquid crystal SLM (LC-SLM) as the mask generator to dynamically generate the slice pattern of each layer. The advantages of this method lie within its simplicity and high throughput. First, the 3D parts are fabricated by simply changing the pattern displayed on the SLM; second, the throughput is much greater than that of the traditional point-scanning manufacturing means. Nevertheless, some drawbacks remain. First, the contrast of the projection pattern is low, and the power needs to be controlled precisely to avert the polymerization in the "dark" region of the pattern. Second, the throughput of the printing system is limited by the refresh rate of the LC-SLM, i.e., ~60 Hz. As discussed previously, DMDs have been frequently used to overcome the speed limitation of LC-SLMs. For example, Sun *et al.* proposed a high-speed PμSL by using the DMD as the dynamic mask generator in 2005 [106]. Due to its good performance, PμSL has been extensively applied in the field of bioengineering [107], metamaterial [25], optics [108], and so on. Although the layer-scanning fabrication method is simple and fast, it has some inherent drawbacks. One is that the maximum throughput of the system is limited by the projection speed, which is determined by the refresh rate of the device, e.g., up to 22.7 kHz for DMD. Another one is that the total voxels in a printed layer are limited by the pixels of the mask. Therefore, certain breakthroughs need to be made to further

improve the throughput, resolution, and diversification of the printing materials.

Nowadays, numerous materials can be used for 3D printing via photopolymerization. 3D objects can be fabricated with hybrid materials by doping different materials into the photoresist, such as metals [109], carbon nanotubes [110], ceramics [111], shape memory polymers [112], hydrogels [113], or composite materials [114]. However, the change of material can lead to process interruption and lengthened processing time, causing structure deformation. Recently, Han *et al.* proposed a rapid multi-material projection microstereolithography (MM-PμSL) by employing dynamic fluidic control of multiple liquid photopolymers within an integrated fluidic cell [115]. Figure 7(a) shows the schematic of the MM-PμSL system and its overall process. In their approach, the LC-SLM was used as the dynamic mask for slice projection. The dynamic fluidic cell enabled the exchange of multiple liquid photopolymers within a few seconds. The 3D structure was thus printed with hybrid material and with high throughput. Figures 7(b)–7(d) demonstrate three different printed structures with hybrid materials: a Taiji symbol patterned with different materials, a bilayer micro-capillary structure with different fluorescent substances, and a 3D helix composed of different metals, respectively. These results indicate that the MM-PμSL technique is suitable for fabricating 3D objects with highly complex structures and multiple materials, which are hardly attainable with other techniques. The prospect for a broader application of this technology is promising, particularly in fields such as bioengineering, functional metamaterials, and micro-robotics.

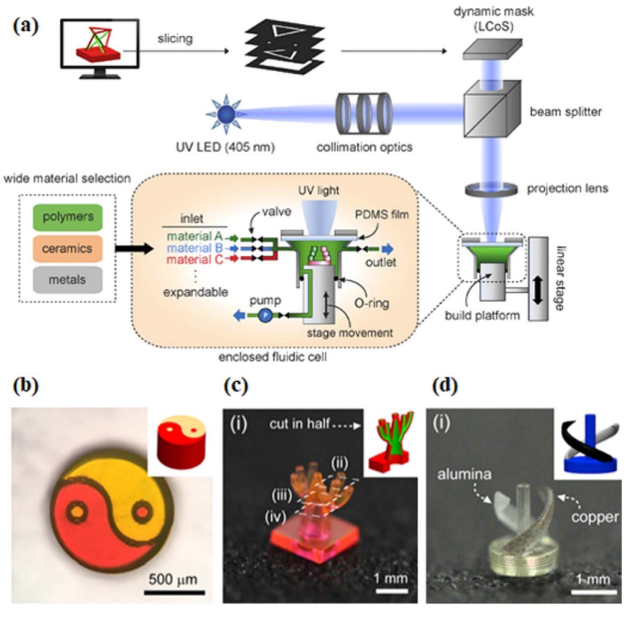

Fig. 7. (a) Schematics of the multi-material projection microstereolithography system and its overall process; (b) Taiji symbol patterned cylinder made of two different materials; (c) multi-material bilayer micro-capillary structure with fluorescent substances; and (d) 3D helix composed of three different parts: particle-free center pillar, two helix arms loaded with copper, and alumina nano-particles (reprinted by permission from Elsevier B.V.: Additive Manufacturing [115], copyright 2019).

In principle, it is challenging to accelerate the printing speed of PμSL to the refresh rate of the dynamic mask, because the exposure, resin renewal, and part movement must be conducted in separate and discrete steps during the fabrication of each layer. In 2015, Tumbleston *et al.* proposed a layer-scanning-based manufacturing method, known as continuous liquid interface production (CLIP), which brought the printing speed close to the refresh rate [68]. The group used the oxygen inhibition to create a reaction "dead zone," or a thin uncured liquid layer, which averted the adhesion between the projection window and the cured part surface. With this method, the printing speed has reached hundreds of millimeters per hour. However, at such a high printing speed, the heat generated by the photopolymerization reaction cannot dissipate timely enough to avoid potential structure deformation. Such a problem could even deteriorate due to the thermal insulation property in the dead zone. Recently, Walker *et al.* proposed a high-area rapid printing (HARP) technique based on the mobile–liquid interface, which allowed continuous printing over large areas [116]. Figure 8(a) illustrates the configuration of the HARP system. A fluorinated oil is used between the projection window and the printed part to reduce the adhesive force in between. The oil is kept at a constant motion speed to further decrease the adhesive force while generating a solid–liquid slip boundary to help dissipate the reaction heat. Figures 8(b) and 8(c) present the velocity profiles and slip boundary flow profiles under the printed part, respectively. A hard-polyurethane acrylate lattice is printed at a size of 30 cm × 30 cm × 30 cm and a resolution of 100 μm in 3 h. The continuous vertical printing speed is 430 mm/h, and the volumetric throughput reaches 100 liters per hour. Potential fields of applications of such continuous printing methods include large-scale prototyping, biocompatible and biodegradable micro-scaffolds, etc., which is useful for both scientific and industrial applications.

The achievable minimum feature size is another area for improvement in the layer-scanning-based additive manufacturing

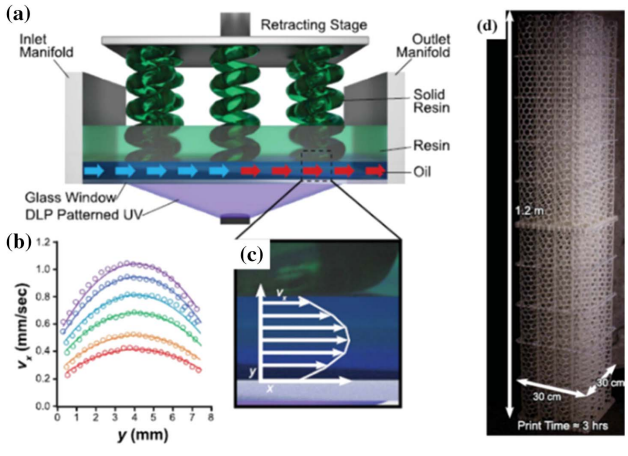

Fig. 8. (a) Schematic for the high-area rapid printing based on mobile–liquid interface; (b) velocity profiles under the printed part at different flow speeds; (c) inset of the slip boundary flow profile under the part; and (d) a ∼1.2-m hard polyurethane acrylate lattice (reprinted by permission from AAAS: Science [116], copyright 2019).

processes, where two-photon polymerization may be a good candidate to reduce the feature size and offset the diffraction limit. To implement two-photon polymerization in a layer-scanning fashion, one cannot directly apply an ultrafast laser to a PμSL system, as it leads to poor axial resolution. In 2005, simultaneous spatial and temporal focusing of femtosecond laser pulses was proposed [117,118], where the laser pulses are first spatially expended by a grating positioned at a focal plane of a 4–*f* system and refocused at the corresponding conjugate plane. The spatial and temporal refocusing occurs only at the conjugate plane, where the dispersed laser spectra are recombined and form a planar light sheet with a thickness of a few micrometers to support two-photon excitation/absorption. With its inherent diffraction property and capability to be rapidly programed, the DMD has been implemented in temporal focusing systems to realize 3D microscopy and laser fabrication applications [119–122]. Recently, our group demonstrated a femtosecond projection two-photon lithography (FP-TPL) technique to achieve scalable sub-micrometer 3D printing based on temporal focusing [123,124], where the DMD simultaneously functions as a blazed grating and programmable mask. Figures 9(a)–9(c) illustrate the formation of programmed femtosecond light sheets and the layer-scanning concept achieved by the FP-TPL, where a layer of the to-be-printed 3D part is generated by programming the designed patterns to the DMD. Figure 9(d) shows various 3D structures printed by the FP-TPL system with the best reported throughput (10–100 mm^3/h), resolution (140/175 nm in the lateral/axial directions), and flexibility. The results indicate that sub-micrometer 3D printing technology is well suited for broad applications in fields such as bioengineering, optics, and healthcare.

As layer-scanning manufacturing systems have optical setups similar to that of a microscope, many emerging imaging methods are readily implementable in the 3D printing system, for example, a 3D printing system inspired by light sheet microscopy [54]. It should be noted that, as all of the layer-scanning and point-scanning manufacturing methods involve stacking the printed layers and voxels to generate a 3D part, this may weaken the mechanical properties of the printed 3D parts along the stacking/printing direction. As such, volumetric manufacturing methods that enable the direct formation of 3D parts in one piece become increasingly appealing.

C. Volumetric Fabrication

Different from the point-scanning and layer-scanning methods, volumetric fabrication means controlling the exposure dose or intensity of every voxel in the whole 3D working space. The 3D object is formed when the intensity or dose at the desired positions exceeds the polymerization threshold. The volumetric fabrication method was first proposed and experimentally demonstrated by Shusteff in 2017 [125]. His group utilized the holographic patterns of light fields to control the intensity in a 3D working space. The laser power was carefully controlled to cure the resin at the desired position with high intensity, thus achieving one-step volumetric additive manufacturing. Figure 10(a) shows the optical configuration of the printing system. The phase-only LC-SLM is used to generate the holographic patterns in x, y, z directions. By using two 45° prisms,

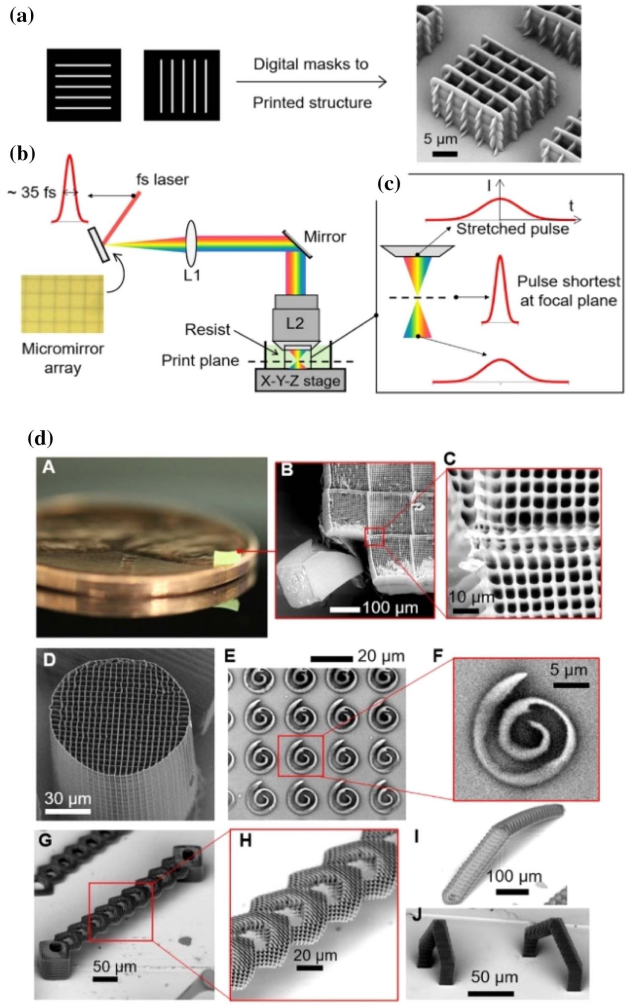

Fig. 9. (a) 3D printing using a layer-by-layer projection of digital masks; (b) optical configuration of the FP-TPL system; (c) zoomed-in schematic of temporal focusing in the focal volume of the objective lens; and (d) structures printed by the FP-TPL system (reprinted by permission from AAAS: Science [123], copyright 2019).

the folded side and bottom beams will meet the central beam in the working space. The intersecting region between the beams will be solidified and a 3D part is formed. The optical attenuation in the resin is also considered to prevent the deformation caused by uneven illumination. Figures 10(b)–10(g) show various aperiodic structures that demonstrate the performance of the printing system. These structures are printed with a single exposure in 5–10 s duration, demonstrating the high throughput characteristic of this technique. While the resolution and size of the fabricated structures are at mesoscale, micro-3D printing can be achieved with the use of a beam delivery system of higher magnification.

Another 3D printing technique successfully derived from advanced microscopy is the volumetric additive manufacturing based on tomographic reconstruction, i.e., computed axial lithography (CAL) [126]. As per the concept of computed tomography [127], the exposure dose of a 3D structure is controlled by illuminating the resin at a constant rotation speed

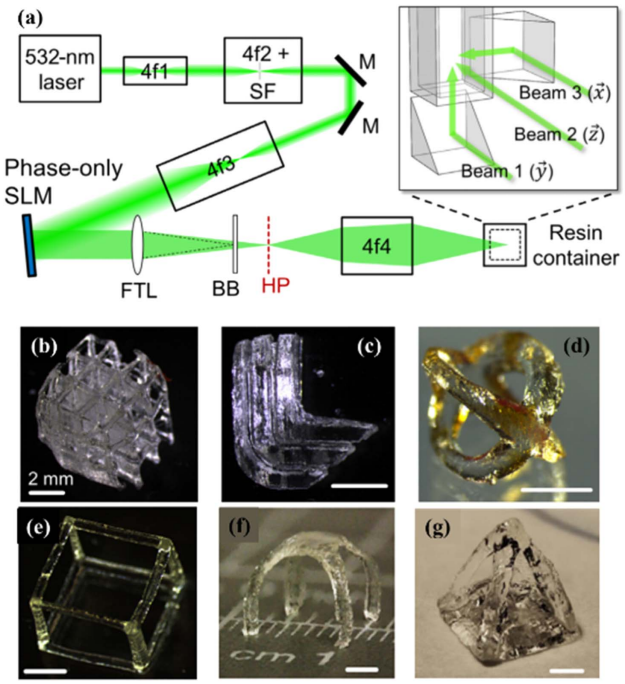

Fig. 10. (a) Optical configuration of the holographic volumetric 3D fabrication system; (b)–(g) structures fabricated with a single exposure (reprinted from AAAS: Science Advances [125], copyright 2017).

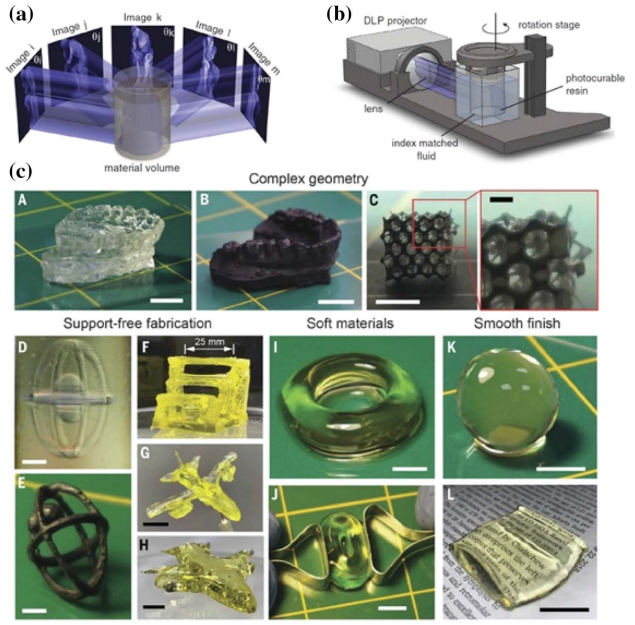

Fig. 11. (a) Printing mechanism of the computed axial lithography; (b) configuration of the computed axial lithography; and (c) various 3D structures printed with different materials (reprinted by permission from AAAS: Science [126], copyright 2019).

with a dynamic light pattern calculated based on the 3D structure. Figures 11(a) and 11(b) show the CAL printing mechanism and system configuration, respectively. Based on the target 3D structure, 2D images are calculated as a function of the rotation angle and serially projected to the rotating resin. To reduce light refraction, the cylindrical resin vat is immersed into the refractive index matching liquid. Figure 11(c) shows a variety of 3D structures fabricated via the CAL system with different materials, which proves the system's fabrication capability for complex and support-free structures and soft materials while obtaining superb surface smoothness. The fabrication time required for these centimeter-scale structures ranges from 30 to 120 s, which attests to the CAL system's high throughput.

In computed tomography, the resolution of the CAL printing system remains limited at 300 μm by the étendue of the light source in the projection process, which is unavoidable and may cause distortion to the printed object. Loterie *et al.* recently proposed a tomographic printing system with higher feature resolution by using a low-étendue illumination system [128]. His group employed an integrated closed-loop feedback system to precisely control the photopolymerization kinetics of the resin in the whole working space to improve the fidelity of the target 3D part. They established a feedback algorithm that considers the influence of light étendue, the viscosity and reactivity of the resin, and the tomographic dose for reconstruction to achieve high resolution and fidelity. Figure 12(a) shows the tomographic 3D fabrication system with feedback achieved by a camera observation system with its light path perpendicular to the printing illumination. In their approach, the camera recorded the images of the build volume in synchronization with the rotation. The images were then sent to the feedback algorithm, and the projection patterns were adjusted accordingly to control the exposure dose. The model in Fig. 12(b) shows that once the feedback is introduced, 3D structures of centimeter scale can be produced in less than 30 s, while obtaining 80 μm positive and 500 μm negative feature sizes. Figure 12(c) shows a comparison between the tomographic 3D printed artery with and without feedback; the results show that the feedback system is conducive to improved printing fidelity.

In comparison with the point-scanning and layer-scanning methods, the volumetric fabrication method performs well in throughput, fidelity, and surface smoothness, despite limited resolution caused by the integration effect. Nevertheless, this approach leads to a new path for ultrafast production of precise structures at mesoscale, e.g., the applications on functional tissue or organ modeling in the bioengineering field.

Each 3D manufacturing method has its strengths and limitations, subject to users' requirements for throughput, resolution, surface smoothness, repeatability, etc. Here, we provide an overview of these key figures of merit (FOMs), i.e., throughput and resolution, as shown in Fig. 13. The labels of the data point refer to the serial numbers of the corresponding references [68,69,79,87–90,94,104,116,122,123,125,126,128–133]. For the purpose of comparing the throughput of these methods, the volumetric processing rates are calculated under the condition in which an all-solid cuboid of the same size is fabricated. It should be noted that random-access point-scanning manufacturing, shown as enlarged green stars in Fig. 13, enjoys some advantages over other point-scanning manufacturing techniques. For example, the fabrication time can be significantly shortened when the to-be-printed structure has a low

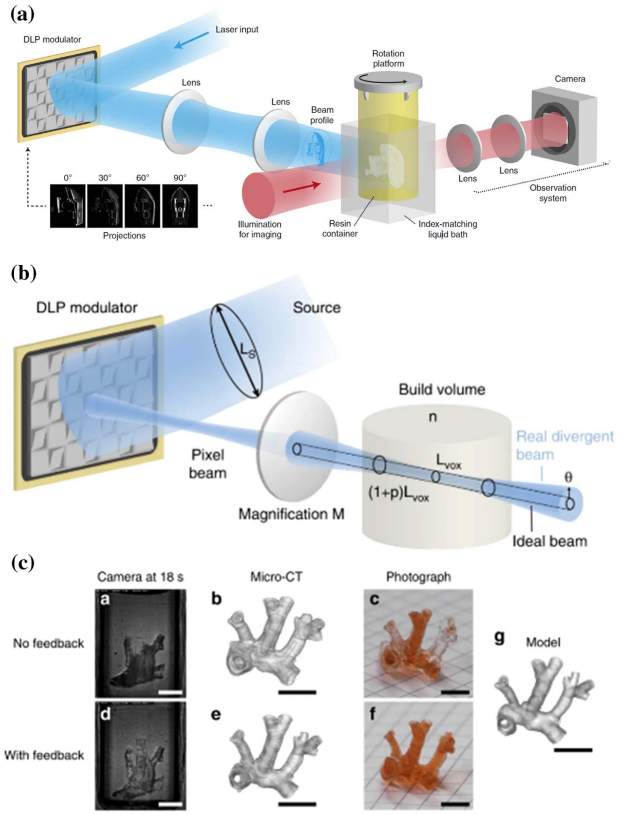

Fig. 12. (a) Configuration of tomographic 3D fabrication system with feedback; (b) étendue-limited optical resolution; and (c) comparison between the tomographic 3D printed artery with and without feedback (reprinted from Springer Nature: Nature Communications [128], copyright 2020).

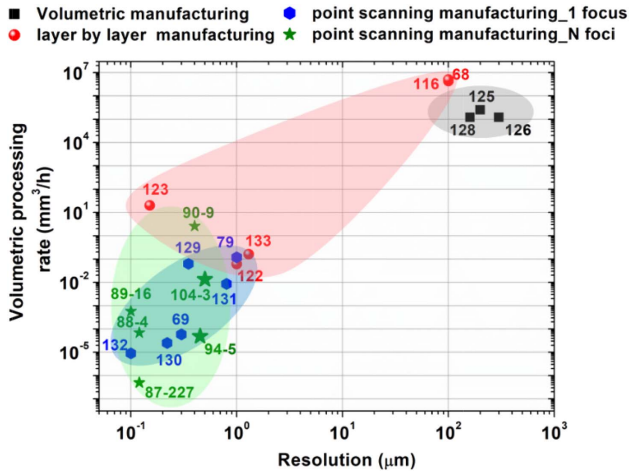

Fig. 13. Summary of different 3D printing techniques plotted versus the resolution (lower logarithmic horizontal scale) and throughput, evaluated with volumetric processing rate (left logarithmic vertical scale): volumetric fabrication (black squares); layer-scanning-based manufacturing (red spheres); single-focus point-scanning fabrication (blue hexagons); multi-focus point-scanning fabrication (green stars); and multi-focus random-access fabrication (enlarged green stars). The labels of the data point refer to the serial numbers of corresponding references. For multi-focus fabrication, the number of foci used is reported next to the reference number after the hyphen.

fill factor, e.g., mechanical metamaterial structures, as time is spent on solidifying only the desired voxels.

4. CRITICAL TOPICS OF INTEREST FOR ADVANCED MICRO-3D PRINTING TECHNIQUES

The FOMs of micro-3D printing technology include resolution, throughput, etc. In principle, the resolution is determined by the NA of the illumination system, and the throughput is determined by the scanning speed and solidification time of the photoresin. In the past few decades, researchers have strived to improve these FOMs, seeking solutions to two specific issues: first, breaking the diffraction limit on printing small features, and second, eliminating the stitching errors associated with large parts. In this section, we will address these determining issues that affect the FOMs of 3D printing techniques.

A. Breaking the Diffraction Limit on Printing Small Features

In the recent development of additive-manufacturing, the fabrication of objects with feature sizes at sub-micrometer scale is critical and extensively investigated. As of today, numerous methods have been proposed. Notable methods include precise power control, two-photon polymerization, and STED-lithography [45,53,56,122]; Figs. 14(a)–14(c) show the mechanisms for printing objects with sub-diffraction limit feature size with a focused light spot in the photoresist using the same optical system. For power control, as the polymer solidification threshold is constant, the feature size of the cured polymer reduces with the decrease in the precisely controlled power [53,122,134]. Although this method effectively trades fabrication rate for resolution, it can be challenging to maintain the uniformity for features smaller than 100 nm in size. As to two-photon polymerization, the exposure dose of the spot is proportional to the square of the intensity. Hence, the feature size is approximately halved compared to linear absorption and a fixed exposure time [3,8,13,44,45,135,136]. STED-lithography has been widely investigated in recent years [53,56,137–139]. As shown in Fig. 14(c), STED-lithography employs one laser to excite pho-

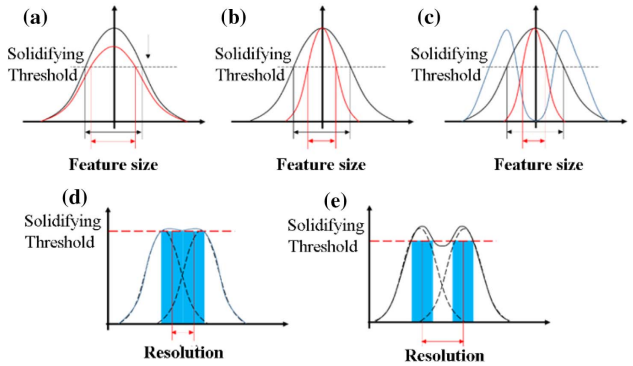

Fig. 14. Illustration of different methods for printing objects with super-resolution feature sizes: (a) precise power control; (b) two-photon polymerization; and (c) STED-lithography: intensity profiles of the polymerization light (black) and depletion light (blue), and exposure-dose profile (red). Definition of resolution by (d) Sparrow limit and (e) Rayleigh limit.

toinitiators for polymerization, and another laser donut spot to locally inhibit the polymerization around the outer rim of the first laser spot [140]. These methods prove to be simple, flexible, and effective for fabricating sparse nanowires. Although STED-lithography calls for more complex and expensive optical systems, it does not compromise the throughput.

It is worth to note that while a smaller feature size is achieved, higher resolution is not always guaranteed. As defined by Abbe, the lateral resolution is the smallest period of a grating that can be distinguished by a microscope with a finite aperture. In other words, to retain the information of the grating period, at least the zeroth- and first-order diffractions need to be collected by the aperture of the objective lens [139]. Figures 14(d) and 14(e) show the resolutions defined by Sparrow and Rayleigh criteria, respectively. The diffraction limit is determined once the optical system is fixed. However, one must note that while the resolution of an image is limited by diffraction, the minimum feature size of an object can break the diffraction limit by precise power control. In other words, the resolution of a point-scanning-based 3D printing system can be improved beyond the diffraction limit by the aforementioned methods as long as the corresponding beam steering device has sufficient scanning resolution. As to projection-based 3D printing systems, the pattern density is constrained by the diffraction limit; yet the minimum feature size can still be engineered to achieve super-resolution. In general, the typical resolution obtained via STED and two-photon polymerization is about 100 nm [45,138]. By adopting the abovementioned methods in one system, it is feasible to achieve a smaller feature size and higher resolution simultaneously [141]. Gan *et al.* has presented a 3D optical beam lithography system achieving a 9 nm feature size and 52 nm resolution in a custom-developed photoresin. This method shows that a properly designed P3DP system can achieve a resolution fully comparable to that of electron beam lithography [53]. In addition to optical methods, the resolution and feature size are subject to an improvement in the photonresin, particularly in the case of two-photon and STED-lithography [142,143]. Hence, a further enhanced P3DP system is expectedly an area for further investigation by both the optical and material communities.

B. Achieving Large-Scale Micro-Additive Manufacturing

Another critical subject matter is undoubtedly large-scale micro-additive manufacturing, i.e., fabrication methods for 3D structures of centimeter scale and micro/nanoscale resolution. In principle, the fabrication of mesoscale 3D parts via photopolymerization can be achieved by volumetric, mechanical point-scanning, and hybrid scanning manufacturing, but each has its challenges apropos of large-scale manufacturing. The volumetric manufacturing approach bears the issue of low resolution. On the other hand, the mechanical point-scanning method is not only time consuming, but also suffers from deformation when scanning continuously at high speed. The hybrid scanning manufacturing, e.g., a combination of an XYZ stage and galvo-scanners, which combines the strengths of optical scanning in precision and speed and that of mechanical scanning at large-motion scale, is seemingly ideal for large-scale high throughput micro-3D printing. Nevertheless, stitching errors may still exist between the 3D elements, and that can potentially weaken the entire structure and compromise the expected mechanical or optical properties. In the following section, we will address the leading causes of and solutions to stitching errors.

First, when two scanning methods are employed simultaneously, stitching errors can occur when their respective coordinates misalign, as each one of them has three degrees of freedom. As the errors continue to accumulate, stitches emerge between the adjacent 3D parts. A potential solution is via real-time position correction. However, it is hardly attainable in practice because errors of such small scale require a stage with extremely high precision [144]. To overcome the barrier, Jonušauskas *et al.* proposed a mesoscale sub-micrometer 3D printing technique using continuous scanning via the synchronization of the galvo-scanners and linear stage [145]. With a complex synchronization algorithm, the linear motion is assigned to the optical and mechanical scanning. The stitching errors are then cleverly apportioned to the whole structure. Figure 15(a) compares the printed mesoscale structures via different scanning methods. The results indicate that the synchronization of the linear stage and galvanometric scanners attains a stitch-free, large-scale, and distortionless structure with high throughput. Figure 15(b) shows various mesoscale structures with sub-micrometer resolution fabricated via this system, where a voxel volume of 0.17 μm^3 and throughput of 32,609 voxels/s have been demonstrated.

Second, the stitches occur when the photoresist shrinks, and the shrinkage leads to the deformation of the 3D parts. With the structure fixed to the substrate, the deformation worsens at locations that are farther from the substrate, as illustrated in Fig. 15(c) [146]. Moreover, the proximity of the two 3D parts is another cause for stitches [147]. The reason is that when stitching two 3D parts, the laser spot is modulated by the cured part, and the printing of the second 3D part is affected as a result, as shown in Fig. 15(c). By optimizing printing strategies, these two setbacks can be resolved [146]. When printing a large-scale object, a better strategy is to fabricate and stitch the printing elements in the horizontal, rather than vertical, direction to circumvent the issue of deformation. It should be noted that the stitching parameters can also be optimized with an ideal diffusion rate and concentration of the photoresin, thereby avoiding the impact of the memory effect of the stitching area on the results [147].

In addition to the aforementioned techniques, we propose two feasible methods for stitch-free, large-scale 3D printing with sub-micrometer resolution. The first approach is to control the dose or structure of the laser spots by light field modulation, e.g., Gerchberg–Saxton algorithm [104,148–151]. The optimization parameters may vary in accordance with the geometric structure of the printed part at the stitching area. The second approach is to correct the scanning errors by introducing a real-time feedback system, where a masked substrate is combined with the image identification technique, to achieve automated highly precise stitching [152,153]. It should be noted that these two methods highly demand the operation speed of the algorithm and efficiency of the control system,

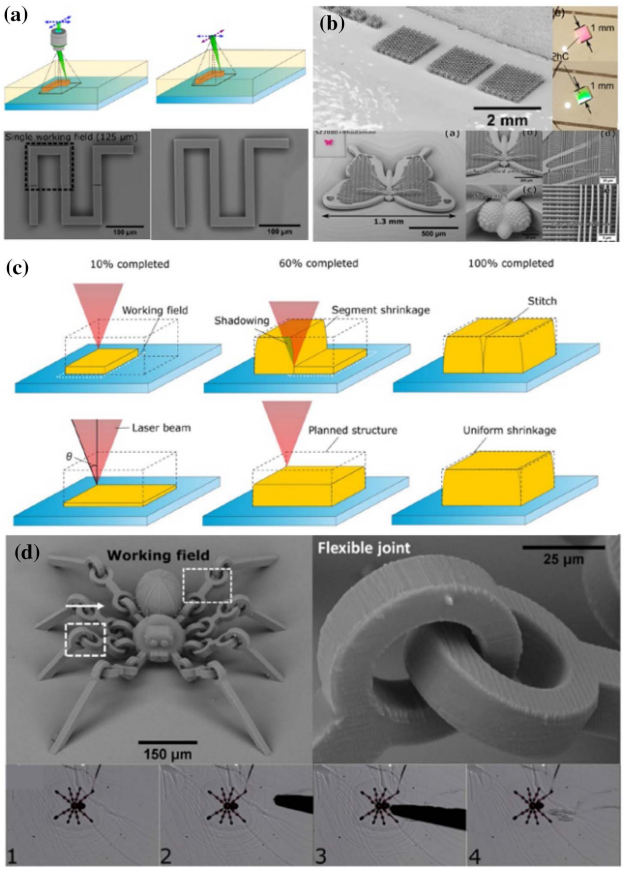

Fig. 15. Mesoscale sub-micrometer 3D printing: (a) mesoscale structures printed via different scanning methods and (b) structures printed by the synchronization of the galvo-scanner and linear stage (reprinted by permission from OSA: Optics Express [145], copyright 2019). (c) Optimized printing strategy against the shrinkage and proximity effect and (d) printed structures after optimization (reprinted from Springer Nature: Scientific Reports [146], copyright 2019).

and may affect the scanning speed. More studies are still needed to explore the benefits of these techniques.

5. CONCLUSION AND OUTLOOK

This paper presents an up-to-date review over emerging micro-3D printing technologies achieved by different optical methods to readers in the optical community. The rapid development of micro-3D printing technologies has revolutionized the manufacturing of micro- to mesoscale products and devices, where P3DP has become one of the most important and fast-developing approaches to micro-3D printing due to its demonstrated advantages in performance and cost effectiveness. In the review, we have systematically examined the performance of different optical-based printing systems, from serial scanning and layer scanning to volumetric manufacturing, with an emphasis on the throughput and resolution. We have also discussed specific challenges in the fabrication of structures with sub-diffraction limit features and in the sub-micrometer manufacturing of large-scale parts. The P3DP technologies may continue to evolve and refine to address the aforementioned challenges via the following means. First, the adaptation of advanced microscopy methods to 3D printing systems, which has been proved to be effective. For example, methods in fluorescent microscopy (e.g., STED, light sheet imaging, random-access scanning) and computerized tomography have been successfully implemented in various 3D printing systems. Second, the development of new printable materials, which helps improve the efficiency of photoresist and quality of the printed structures. In addition, the development of functional photoresins may enable functional devices to be printed directly, e.g., piezoelectric sensor arrays. Finally, new and innovative methods in the optical fields, which are the main driver of scientific development. We foresee many of the emerging P3DP technologies discussed in this paper to be adopted and scaled up for practical applications and to impact the engineering industry in the near future.

Funding. National Natural Science Foundation of China (11904180); Research Grants Council, University Grants Committee (14203020, 14209018); Innovation and Technology Fund (ITS/196/19FP).

Disclosures. The authors declare no conflicts of interest.

REFERENCES

1. S. Y. Chou, P. R. Krauss, and P. J. Renstrom, "Imprint of sub-25 nm vias and trenches in polymers," Appl. Phys. Lett. **67**, 3114–3116 (1995).
2. J. Chen, C. Gu, H. Lin, and S. Chen, "Soft mold-based hot embossing process for precision imprinting of optical components on nonplanar surfaces," Opt. Express **23**, 20977–20985 (2015).
3. B. Berman, "3-D printing: the new industrial revolution," Bus. Horizons **55**, 155–162 (2012).
4. J. W. Stansbury and M. J. Idacavage, "3D printing with polymers: challenges among expanding options and opportunities," Dent. Mater. **32**, 54–64 (2016).
5. C. Barner-Kowollik, M. Bastmeyer, E. Blasco, G. Delaittre, P. Mgller, B. Richter, and M. Wegener, "3D laser micro- and nanoprinting: challenges for chemistry," Angew. Chem. **56**, 15828–15845 (2017).
6. F. Rengier, A. Mehndiratta, H. V. Tenggkobligk, C. M. Zechmann, R. Unterhinninghofen, H. Kauczor, and F. L. Giesel, "3D printing based on imaging data: review of medical applications," Int. J. Comput. Ass. Rad. **5**, 335–341 (2010).
7. G. H. Wu and S. H. Hsu, "Review: polymeric-based 3D printing for tissue engineering," J. Med. Biol. Eng. **35**, 285–292 (2015).
8. J. Xing, M. Zheng, and X. Duan, "Two-photon polymerization microfabrication of hydrogels: an advanced 3D printing technology for tissue engineering and drug delivery," Chem. Soc. Rev. **44**, 5031–5039 (2015).
9. R. D. Sochol, E. C. Sweet, C. C. Glick, S. Wu, C. Yang, M. A. Restaino, and L. Lin, "3D printed microfluidics and microelectronics," Microelectron. Eng. **189**, 52–68 (2018).
10. J. A. Lewis and B. Y. Ahn, "Device fabrication: three-dimensional printed electronics," Nature **518**, 42–43 (2015).
11. Y. L. Kong, I. A. Tamargo, H. Kim, B. N. Johnson, M. K. Gupta, T. Koh, H. Chin, D. A. Steingart, B. P. Rand, and M. C. Mcalpine, "3D printed quantum dot light-emitting diodes," Nano Lett. **14**, 7017–7023 (2014).
12. T. Gissibl, S. Thiele, A. M. Herkommer, and H. Giessen, "Two-photon direct laser writing of ultracompact multi-lens objectives," Nat. Photonics **10**, 554–560 (2016).
13. B. H. Cumpston, S. P. Ananthavel, S. Barlow, D. L. Dyer, J. E. Ehrlich, L. Erskine, A. A. Heikal, S. M. Kuebler, I. Y. S. Lee, D. Mccordmaughon, J. Qin, H. Rockel, M. Rumi, X. L. Wu, S. R. Marder, and J. W. Perry, "Two-photon polymerization initiators for

three-dimensional optical data storage and microfabrication," Nature **398**, 51–54 (1999).
14. P.-I. Dietrich, M. Blaicher, I. Reuter, M. Billah, T. Hoose, A. Hofmann, C. Caer, R. Dangel, B. Offrein, U. Troppenz, M. Moehrle, W. Freude, and C. Koos, "*In situ* 3D nanoprinting of free-form coupling elements for hybrid photonic integration," Nat. Photonics **12**, 241–247 (2018).
15. J. Luo, L. J. Gilbert, D. A. Bristow, R. G. Landers, J. T. Goldstein, A. M. Urbas, and E. C. Kinzel, "Additive manufacturing of glass for optical applications," Proc. SPIE **9738**, 97380Y (2016).
16. Y. AbouHashem, M. Dayal, S. Savanah, and G. Štrkalj, "The application of 3D printing in anatomy education," Med. Educ. Online **20**, 29847 (2015).
17. C. Gosselin, R. Duballet, P. Roux, N. Gaudilliere, J. Dirrenberger, and P. Morel, "Large-scale 3D printing of ultra-high-performance concrete—a new processing route for architects and builders," Mater. Design **100**, 102–109 (2016).
18. C. Yeh and Y. Chen, "Critical success factors for adoption of 3D printing," Technol. Forecast. Soc. **132**, 209–216 (2018).
19. Grand View Research, "3D printing market size, share & trends analysis report by material, by component, by printer type, by technology, by software, by application, by vertical, and segment forecasts, 2020–2027," Market Research Report (2020).
20. M. Vaezi, H. Seitz, and S. Yang, "A review on 3D micro-additive manufacturing technologies," Int. J. Adv. Manuf. Technol. **67**, 1721–1754 (2013).
21. R. D. Sochol, E. Sweet, C. C. Glick, S. Venkatesh, A. Avetisyan, K. F. Ekman, A. Raulinaitis, A. Tsai, A. Wienkers, K. Korner, K. Hanson, A. Long, B. J. Hightower, G. Slatton, D. C. Burnett, T. L. Massey, K. Iwai, L. P. Lee, K. S. J. Pister, and L. Lin, "3D printed microfluidic circuitry via multijet-based additive manufacturing," Lab Chip **16**, 668–678 (2016).
22. S. Wong, M. Deubel, F. Pérez-Willard, S. John, G. A. Ozin, M. Wegener, and G. von Freymann, "Direct laser writing of three-dimensional photonic crystals with a complete photonic bandgap in chalcogenide glasses," Adv. Mater. **18**, 265–269 (2006).
23. F. Klein, B. Richter, T. Striebel, C. M. Franz, G. von Freymann, M. Wegener, and M. Bastmeyer, "Two-component polymer scaffolds for controlled three-dimensional cell culture," Adv. Mater. **23**, 1341–1345 (2011).
24. J. J. Adams, E. B. Duoss, T. F. Malkowski, M. J. Motala, B. Y. Ahn, R. G. Nuzzo, J. T. Bernhard, and J. A. Lewis, "Conformal printing of electrically small antennas on three-dimensional surfaces," Adv. Mater. **23**, 1335–1340 (2011).
25. X. Zheng, H. Lee, T. H. Weisgraber, M. Shusteff, J. DeOtte, E. B. Duoss, J. D. Kuntz, M. M. Biener, Q. Ge, J. A. Jackson, S. O. Kucheyev, N. X. Fang, and C. M. Spadaccini, "Ultralight, ultrastiff mechanical metamaterials," Science **344**, 1373–1377 (2014).
26. N. Zhou, C. Liu, J. A. Lewis, and D. Ham, "Gigahertz electromagnetic structures via direct ink writing for radio-frequency oscillator and transmitter applications," Adv. Mater. **29**, 1605198 (2017).
27. M. A. Jafari, W. Han, F. Mohammadi, A. Safari, S. C. Danforth, and N. A. Langrana, "A novel system for fused deposition of advanced multiple ceramics," Rapid Prototyping J. **6**, 161–175 (2000).
28. T. B. F. Woodfield, J. Malda, J. de Wijn, F. Péters, J. Riesle, and C. A. Van Blitterswijk, "Design of porous scaffolds for cartilage tissue engineering using a three-dimensional fiber-deposition technique," Biomaterials **25**, 4149–4161 (2004).
29. R. J. A. Allen and R. S. Trask, "An experimental demonstration of effective curved layer fused filament fabrication utilising a parallel deposition robot," Addit. Manuf. **8**, 78–87 (2015).
30. J. Go, S. N. Schiffres, A. G. Stevens, and A. JohnHart, "Rate limits of additive manufacturing by fused filament fabrication and guidelines for high-throughput system design," Addit. Manuf. **16**, 1–11 (2017).
31. K. K. B. Hon, L. Li, and I. M. Hutchings, "Direct writing technology-advances and developments," CIRP Ann. **57**, 601–620 (2008).
32. G. M. Gratson, M. Xu, and J. A. Lewis, "Direct writing of three-dimensional webs," Nature **428**, 386 (2004).
33. E. B. Duoss, T. H. Weisgraber, K. Hearon, C. Zhu, W. Small, T. R. Metz, J. J. Vericella, H. D. Barth, J. D. Kuntz, R. S. Maxwell, C. M. Spadaccini, and T. S. Wilson, "Three-dimensional printing of elastomeric, cellular architectures with negative stiffness," Adv. Funct. Mater. **24**, 4905–4913 (2014).
34. T. D. Ngo, A. Kashania, G. Imbalzano, K. T. Q. Nguyen, and D. Hui, "Additive manufacturing (3D printing): a review of materials, methods, applications and challenges," Composites Part B **143**, 172–196 (2018).
35. D. J. Ryu, C. Sonn, D. H. Hong, K. B. Kwon, S. J. Park, H. Y. Ban, T. Y. Kwak, D. Lim, and J. H. Wang, "Titanium porous coating using 3D direct energy deposition (DED) printing for cementless TKA implants: does it induce chronic inflammation?" Materials **13**, 472 (2020).
36. L. Hirt, A. Reiser, R. Spolenak, and T. Zambelli, "Additive manufacturing of metal structures at the micrometer scale," Adv. Mater. **29**, 1604211 (2017).
37. J. D. Fowlkes, R. Winkler, B. B. Lewis, A. Fernández-Pacheco, L. Skoric, D. Sanz-Hernández, M. G. Stanford, E. Mutunga, P. D. Rack, and H. Plank, "High-fidelity 3D-nanoprinting via focused electron beams: computer-aided design (3BID)," ACS Appl. Nano Mater. **1**, 1028–1041 (2018).
38. J. Kechagias, "An experimental investigation of the surface roughness of parts produced by LOM process," Rapid Prototyping J. **13**, 17–22 (2007).
39. D. X. Luong, A. K. Subramanian, G. A. Lopez Silva, J. Yoon, S. Cofer, K. Yang, P. S. Owuor, T. Wang, Z. Wang, J. Lou, P. M. Ajayan, and J. M. Tour, "Laminated object manufacturing of 3D-printed laser-induced graphene foams," Adv. Mater. **30**, 1707416 (2018).
40. A. Reiser, M. Linden, P. Rohner, A. Marchand, H. Galinski, A. S. Sologubenko, J. M. Wheeler, R. Zenobi, D. Poulikakos, and R. Spolenak, "Multi-metal electrohydrodynamic redox 3D printing at the submicron scale," Nat. Commun. **10**, 1853 (2019).
41. J. Schneider, P. Rohner, D. Thureja, M. Schmid, P. Galliker, and D. Poulikakos, "Electrohydrodynamic nano drip printing of high aspect ratio metal grid transparent electrodes," Adv. Funct. Mater. **26**, 833–840 (2016).
42. S. A. Khairallah, A. T. Anderson, A. M. Rubenchik, and W. E. King, "Laser powder-bed fusion additive manufacturing physics of complex melt flow and formation mechanisms of pores, spatter, and denudation zones," Acta Mater. **108**, 36–45 (2016).
43. F. Fina, S. Gaisford, and A. W. Basit, "Powder bed fusion: the working process, current applications and opportunities," in *3D Printing of Pharmaceuticals*, A. Basit and S. Gaisford, eds., Vol. **31** of AAPS Advances in the Pharmaceutical Sciences Series (Springer, 2018), pp. 81–105.
44. S. Maruo, O. Nakamura, and S. Kawata, "Three-dimensional microfabrication with two-photon-absorbed photopolymerization," Opt. Lett. **22**, 132–134 (1997).
45. S. Kawata, H. B. Sun, T. Tanaka, and K. Takada, "Finer features for functional microdevices–micromachines can be created with higher resolution using two-photon absorption," Nature **412**, 697–698 (2001).
46. T. Gissibl, S. Thiele, A. M. Herkommer, and H. Giessen, "Sub-micrometre accurate free-form optics by three-dimensional printing on single-mode fibres," Nat. Commun. **7**, 11763 (2016).
47. R. Raman, B. Bhaduri, M. Mir, A. Shkumatov, M. K. Lee, G. Popescu, H. Kong, and R. Bashir, "High-resolution projection microstereolithography for patterning of neovasculature," Adv. Health Mater. **5**, 610–619 (2016).
48. D. J. Mcgregor, S. H. Tawfick, and W. P. King, "Mechanical properties of hexagonal lattice structures fabricated using continuous liquid interface production additive manufacturing," Addit. Manuf. **25**, 10–18 (2019).
49. K. William, J. Maxwell, K. Larsson, and M. Boman, "Freeform fabrication of functional microsolenoids, electromagnets and helical springs using high pressure laser chemical vapour deposition," in *Proceedings of the 12th IEEE International Conference on Micro Electro Mechanical Systems (MEMS)* (IEEE, 1999), pp. 232–237.
50. M. C. Wanke, O. Lehmann, K. Muller, Q. Wen, and M. Stuke, "Laser rapid prototyping of photonic band-gap microstructures," Science **275**, 1284–1286 (1997).
51. E. Saleh, P. Woolliams, B. Clarke, A. Gregory, S. Greedy, C. Smartt, R. D. Wildman, I. A. Ashcroft, R. J. M. Hague, P. Dickens, and

C. Tuck, "3D inkjet-printed UV-curable inks for multi-functional electromagnetic applications," Addit. Manuf. **13**, 143–148 (2017).
52. E. B. Duoss, M. Twardowski, and J. A. Lewis, "Sol-gel inks for direct-write assembly of functional oxides," Adv. Mater. **19**, 3485–3489 (2007).
53. Z. Gan, Y. Cao, R. A. Evans, and M. Gu, "Three-dimensional deep sub-diffraction optical beam lithography with 9 nm feature size," Nat. Commun. **4**, 2061 (2013).
54. V. Hahn, F. Mayer, M. Thiel, and M. Wegener, "3-D laser nanoprinting," Opt. Photon. News **30**, 28–35 (2019).
55. S. W. Hell and J. Wichmann, "Breaking the diffraction resolution limit by stimulated emission: stimulated-emission-depletion fluorescence microscopy," Opt. Lett. **19**, 780–782 (1994).
56. J. Fischer and M. Wegener, "Three-dimensional optical laser lithography beyond the diffraction limit," Laser Photon. Rev. **7**, 22–44 (2013).
57. D. L. Forman, M. C. Cole, and R. R. McLeod, "Radical diffusion limits to photo inhibited super resolution lithography," Phys. Chem. Chem. Phys. **15**, 14862–14867 (2013).
58. E. Andrzejewska, "Photo polymerization kinetics of multifunctional monomers," Prog. Polym. Sci. **26**, 605–665 (2001).
59. R. F. T. Stepto, J. I. Cail, and D. J. R. Taylor, "Polymer networks: principles of formation, structure and properties," Polimery Warsaw **45**, 455–464 (2000).
60. E. Andrzejewska, M. B. Bogacki, and M. Andrzejewski, "Variations of rate coefficients and termination mechanism during the after-effects of a light-induced polymerization of a dimethacrylate monomer," Macromol. Theor. Simul. **10**, 842–849 (2001).
61. S. Zhu and A. Hamielec, "Kinetics of polymeric network synthesis via free-radical mechanisms-polymerization and polymer modification," Makromolekulare Chemie. Macromolecular Symposia. **63**, 135–182 (1992).
62. O. George, *Principles of Polymerization* (Wiley, 2004).
63. X. Allonas, J. Lalevee, F. Morlet-Savary, and J. P. Fouassier, "Understanding the reactivity of photo initiating systems for photo polymerization," Polimery **51**, 491–498 (2006).
64. G. W. Sluggett, P. F. Mcgarry, I. V. Koptyug, and N. J. Turro, "Laser flash photolysis and time-resolved ESR study of phosphinoyl radical structure and reactivity," J. Am. Chem. Soc. **118**, 7367–7372 (1996).
65. U. Kolczak, G. Rist, K. Dietliker, and J. Wirz, "Reaction mechanism of monoacyl- and bisacylphosphine oxide photoinitiators studied by ^{31}P-, ^{13}C-, and ^{1}H-CIDNP and ESR," J. Am. Chem. Soc. **118**, 6477–6489 (1996).
66. M. Rumi, S. Barlow, J. Wang, J. W. Perry, and S. R. Marder, "Two-photon absorbing materials and two-photon-induced chemistry," in *Photoresponsive Polymers* (Springer, 2008), pp. 1–95.
67. S. Maruo and K. Ikuta, "Submicron stereolithography for the production of freely movable mechanisms by using single-photon polymerization," Sens. Actuators A **100**, 70–76 (2002).
68. J. R. Tumbleston, D. Shirvanyants, N. Ermoshkin, R. Janusziewicz, A. R. Johnson, D. L. Kelly, K. Chen, R. K. Pinschmidt, J. P. Rolland, A. Ermoshkin, E. T. Samulski, and J. M. Desimone, "Continuous liquid interface production of 3D objects," Science **347**, 1349–1352 (2015).
69. J. Fischer, J. B. Mueller, J. Kaschke, T. J. A. Wolf, A. N. Unterreiner, and M. Wegener, "Three-dimensional multi-photon direct laser writing with variable repetition rate," Opt. Express **21**, 26244–26260 (2013).
70. M. Malinauskas, V. Purlys, M. Rutkauskas, A. Gaidukevičiūtė, and R. Gadonas, "Femtosecond visible light induced two-photon photopolymerization for 3D micro/nanostructuring in photoresists and photopolymers," Lith. J. Phys. **50**, 201–207 (2010).
71. I. Sakellari, E. Kabouraki, D. Gray, V. Purlys, C. Fotakis, A. Pikulin, N. Bityurin, M. Vamvakaki, and M. Farsari, "Diffusion-assisted high-resolution direct femtosecond laser writing," ACS Nano **6**, 2302–2311 (2012).
72. J. Zhang and P. Xiao, "3D printing of photopolymers," Polym. Chem. **9**, 1530–1540 (2018).
73. X. Fan, Y. Huang, X. Ding, N. Luo, C. Li, N. Zhao, and S. Chen, "Alignment-free liquid capsule pressure sensor for cardiovascular monitoring," Adv. Funct. Mater. **28**, 1805045 (2018).
74. H. Cui, R. Hensleigh, D. Yao, D. Maurya, P. Kumar, M. G. Kang, S. Priya, and X. R. Zheng, "Three-dimensional printing of piezoelectric materials with designed anisotropy and directional response," Nat. Mater. **18**, 234–241 (2019).
75. A. Marino, C. Filippeschi, V. Mattoli, B. Mazzolai, and G. Ciofani, "Biomimicry at the nanoscale: current research and perspectives of two-photon polymerization," Nanoscale **7**, 2841–2850 (2015).
76. M. T. Gale, M. Rossi, J. Pedersen, and H. Schuetz, "Fabrication of continuous-relief micro-optical elements by direct laser writing in photoresists," Opt. Eng. **33**, 3556–3566 (1994).
77. A. Selimis, V. Mironov, and M. Farsari, "Direct laser writing: principles and materials for scaffold 3D printing," Microelectron. Eng. **132**, 83–89 (2015).
78. M. Malinauskas, P. Danilevičius, and S. Juodkazis, "Three-dimensional micro-/nano-structuring via direct write polymerization with picosecond laser pulses," Opt. Express **19**, 5602–5610 (2011).
79. B. W. Pearre, C. Michas, J. Tsang, T. J. Gardner, and T. M. Otchy, "Fast micron-scale 3D printing with a resonant-scanning two-photon microscope," Addit. Manuf. **30**, 100887 (2019).
80. K. Obata, A. Eltamer, L. Koch, U. Hinze, and B. N. Chichkov, "High-aspect 3D two-photon polymerization structuring with widened objective working range (WOW-2PP)," Light Sci. Appl. **2**, e116 (2013).
81. W. Chu, Y. Tan, P. Wang, J. Xu, W. Li, J. Qi, and Y. Cheng, "Centimeter-height 3D printing with femtosecond laser two-photon polymerization," Adv. Mater. Technol. **3**, 1700396 (2018).
82. Y. Kuroiwa, N. Takeshima, Y. Narita, S. Tanaka, and K. Hirao, "Arbitrary micropatterning method in femtosecond laser micro processing using diffractive optical elements," Opt. Express **12**, 1908–1915 (2004).
83. T. Kondo, S. Matsuo, S. Juodkazis, V. Mizeikis, and H. Misawa, "Multi photon fabrication of periodic structures by multi beam interference of femtosecond pulses," Appl. Phys. Lett. **82**, 2758–2760 (2003).
84. L. Kelemen, S. Valkai, and P. Ormos, "Parallel photo polymerisation with complex light patterns generated by diffractive optical elements," Opt. Express **15**, 14488–14497 (2007).
85. K. Obata, J. Koch, U. Hinze, and B. N. Chichkov, "Multi-focus two-photon polymerization technique based on individually controlled phase modulation," Opt. Express **18**, 17193–17200 (2010).
86. X. Chen, Y. Song, W. Zhang, M. Sulaman, S. Zhao, B. Guo, Q. Hao, and L. Li, "Imaging method based on the combination of microlens arrays and aperture arrays," Appl. Opt. **57**, 5392–5398 (2018).
87. J. Kato, N. Takeyasu, Y. Adachi, H. Sun, and S. Kawata, "Multiple-spot parallel processing for laser micro nanofabrication," Appl. Phys. Lett. **86**, 044102 (2005).
88. X. Dong, Z. Zhao, and X. Duan, "Micronanofabrication of assembled three-dimensional microstructures by designable multiple beams multiphoton processing," Appl. Phys. Lett. **91**, 124103 (2007).
89. S. D. Gittard, A. Nguyen, K. Obata, A. Koroleva, R. J. Narayan, and B. N. Chichkov, "Fabrication of microscale medical devices by two-photon polymerization with multiple foci via a spatial light modulator," Biomed. Opt. Express **2**, 3167–3178 (2011).
90. V. Hahn, P. Kiefer, T. Frenzel, J. Qu, E. Blasco, C. Barnerkowollik, and M. Wegener, "Rapid assembly of small materials building blocks (voxels) into large functional 3D metamaterials," Adv. Funct. Mater. **30**, 1907795 (2020).
91. T. Bückmann, M. Thiel, M. Kadic, R. Schittny, and M. Wegener, "An elasto-mechanical unfeelability cloak made of pentamode metamaterials," Nat. Commun. **5**, 4130 (2014).
92. L. Yang, A. Eltamer, U. Hinze, J. Li, Y. Hu, W. Huang, J. Chu, and B. N. Chichkov, "Parallel direct laser writing of micro-optical and photonic structures using spatial light modulator," Opt. Laser Eng. **70**, 26–32 (2015).
93. T. Baldacchini, S. Snider, and R. Zadoyan, "Two-photon polymerization with variable repetition rate bursts of femtosecond laser pulses," Opt. Express **20**, 29890–29899 (2012).
94. G. Vizsnyiczai, L. Kelemen, and P. Ormos, "Holographic multi-focus 3D two-photon polymerization with real-time calculated holograms," Opt. Express **22**, 24217–24223 (2014).

95. M. Manousidaki, D. G. Papazoglou, M. Farsari, and S. Tzortzakis, "3D holographic light shaping for advanced multiphoton polymerization," Opt. Lett. **45**, 85–88 (2020).
96. C. Gu, Y. Chang, D. Zhang, J. Cheng, and S. Chen, "Femtosecond laser pulse shaping at megahertz rate via a digital micromirror device," Opt. Lett. **40**, 4018–4021 (2015).
97. J. Cheng, C. Gu, D. Zhang, D. Wang, and S. Chen, "Ultrafast axial scanning for two-photon microscopy via a digital micromirror device and binary holography," Opt. Lett. **41**, 1451–1454 (2016).
98. M. Ren, J. Chen, D. Chen, and S. Chen, "Aberration-free 3D imaging via DMD-based two-photon microscopy and sensorless adaptive optics," Opt. Lett. **45**, 2656–2659 (2020).
99. D. Wang, J. F. C. Loo, W. Lin, Q. Geng, E. K. S. Ngan, S. K. Kong, Y. Yam, S. Chen, and H. P. Ho, "Development of a sensitive DMD-based 2-D SPR sensor array using single-point detection strategy for multiple aptamer screening," Sens. Actuators B **305**, 127240 (2020).
100. D. Wang, C. Wen, Y. Chang, W. Lin, and S. Chen, "Ultrafast laser-enabled 3D metal printing: a solution to fabricate arbitrary submicron metal structures," Precis. Eng. **52**, 106–111 (2018).
101. C. Wen, F. Feng, M. Ren, M. Somek, N. Zhao, and S. Chen, "Spatially-resolved random-access pump-probe microscopy based on binary holography," Opt. Lett. **44**, 4083–4086 (2019).
102. C. Wen, M. Ren, F. Feng, W. Chen, and S. Chen, "Compressive sensing for fast 3-D and random-access two-photon microscopy," Opt. Lett. **44**, 4343–4346 (2019).
103. Q. Geng, C. Gu, J. Cheng, and S. Chen, "Digital micromirror device-based two-photon microscopy for three-dimensional and random-access imaging," Optica **4**, 674–677 (2017).
104. Q. Geng, D. Wang, P. Chen, and S. Chen, "Ultrafast multi-focus 3-D nano-fabrication based on two-photon polymerization," Nat. Commun. **10**, 2179 (2019).
105. A. Bertsch, S. Zissi, J. Y. Jézéquel, S. Corbel, and J. C. Andre, "Microstereophotolithography using a liquid crystal display as dynamic mask-generator," Microsyst. Technol. **3**, 42–47 (1997).
106. C. Sun, N. Fang, D. M. Wu, and X. Zhang, "Projection micro-stereolithography using digital micro-mirror dynamic mask," Sens. Actuators A **121**, 113–120 (2005).
107. J. Choi, R. B. Wicker, S. Lee, K. H. Choi, C. Ha, and I. Chung, "Fabrication of 3D biocompatible/biodegradable micro-scaffolds using dynamic mask projection microstereolithography," J. Mater. Process. Technol. **209**, 5494–5503 (2009).
108. H. Kim, S. K. Moon, and M. Seo, "Hybrid layering scanning-projection micro-stereolithography for fabrication of conical micro-lens array and hollow microneedle array," Microelectron. Eng. **153**, 15–19 (2016).
109. Q. Wang, J. A. Jackson, Q. Ge, J. B. Hopkins, C. M. Spadaccini, and N. X. Fang, "Lightweight mechanical metamaterials with tunable negative thermal expansion," Phys. Rev. Lett. **117**, 175901 (2016).
110. Q. Mu, L. Wang, C. K. Dunn, X. Kuang, F. Duan, Z. Zhang, H. J. Qi, and T. Wang, "Digital light processing 3D printing of conductive complex structures," Addit. Manuf. **18**, 74–83 (2017).
111. X. Song, Y. Chen, T. W. Lee, S. Wu, and L. Cheng, "Ceramic fabrication using mask-image-projection-based stereolithography integrated with tape-casting," J. Manuf. Proc. **20**, 456–464 (2015).
112. Y. Y. C. Choong, S. Maleksaeedi, H. Eng, P.-C. Su, and J. Wei, "Curing characteristics of shape memory polymers in 3D projection and laser stereolithography," Virtual Phys. Prototyp. **12**, 77–84 (2017).
113. D. Han, C. Farino, C. Yang, T. Scott, D. Browe, W. Choi, J. W. Freeman, and H. Lee, "Soft robotic manipulation and locomotion with a 3D printed electroactive hydrogel," ACS Appl. Mater. Interfaces **10**, 17512–17518 (2018).
114. Y. Yang, Z. Chen, X. Song, B. Zhu, T. K. Hsiai, P. Wu, R. Xiong, J. Shi, Y. Chen, Q. Zhou, and K. K. Shung, "Three dimensional printing of high dielectric capacitor using projection based stereolithography method," Nano Energy **22**, 414–421 (2016).
115. D. Han, C. Yang, N. X. Fang, and H. Lee, "Rapid multi-material 3D printing with projection micro-stereolithography using dynamic fluidic control," Addit. Manuf. **27**, 606–615 (2019).
116. D. A. Walker, J. L. Hedrick, and C. A. Mirkin, "Rapid, large-volume, thermally controlled 3D printing using a mobile liquid interface," Science **366**, 360–364 (2019).
117. G. Zhu, J. V. Howe, M. Durst, W. Zipfel, and C. Xu, "Simultaneous spatial and temporal focusing of femtosecond pulses," Opt. Express **13**, 2153–2159 (2005).
118. D. Oron, E. Tal, and Y. Silberberg, "Scanningless depth-resolved microscopy," Opt. Express **13**, 1468–1476 (2005).
119. J. N. Yih, Y. Y. Hu, Y. D. Sie, L. C. Cheng, C. H. Lien, and S. J. Chen, "Temporal focusing based multiphoton excitation microscopy via digital micromirror device," Opt. Lett. **39**, 3134–3137 (2014).
120. Y. Meng, W. Lin, C. Li, and S. Chen, "Fast two-snapshot structured illumination for temporal focusing microscopy with enhanced axial resolution," Opt. Express **25**, 23109–23121 (2017).
121. C. Gu, D. Zhang, D. Wang, Y. Yam, C. Li, and S. Chen, "Parallel femtosecond laser light sheet micro-manufacturing based on temporal focusing," Precis. Eng. **50**, 198–203 (2017).
122. Y. Li, L. Cheng, C. Chang, C. Lien, P. J. Campagnola, and S. J. Chen, "Fast multiphoton microfabrication of freeform polymer microstructures by spatiotemporal focusing and patterned excitation," Opt. Express **20**, 19030–19038 (2012).
123. S. K. Saha, D. Wang, V. H. Nguyen, Y. Chang, J. S. Oakdale, and S. Chen, "Scalable submicrometer additive manufacturing," Science **366**, 105–109 (2019).
124. S. K. Saha and S. Chen, "Comment on 'rapid assembly of small materials building blocks (voxels) into large functional 3D metamaterials'," Adv. Funct. Mater. **30**, 2001060 (2020).
125. M. Shusteff, A. E. M. Browar, B. Kelly, J. Henriksson, T. H. Weisgraber, R. M. Panas, N. X. Fang, and C. M. Spadaccini, "One-step volumetric additive manufacturing of complex polymer structures," Sci. Adv. **3**, eaao5496 (2017).
126. B. Kelly, I. Bhattacharya, H. Heidari, M. Shusteff, C. M. Spadaccini, and H. Taylor, "Volumetric additive manufacturing via tomographic reconstruction," Science **363**, 1075–1079 (2019).
127. D. J. Brenner and E. J. Hall, "Computed tomography—an increasing source of radiation exposure," New Engl. J. Med. **357**, 2277–2284 (2007).
128. D. Loterie, P. Delrot, and C. Moser, "High-resolution tomographic volumetric additive manufacturing," Nat. Commun. **11**, 852 (2020).
129. J. S. Oakdale, R. F. Smith, J. Forien, W. L. Smith, S. Ali, L. B. B. Aji, T. M. Willey, J. Ye, A. W. V. Buuren, M. A. Worthington, S. T. Prisbrey, H. Park, P. Amendt, T. F. Baumann, and J. Biener, "Direct laser writing of low-density interdigitated foams for plasma drive shaping," Adv. Funct. Mater. **27**, 1702425 (2017).
130. L. R. Meza, S. Das, and J. R. Greer, "Strong, lightweight, and recoverable three-dimensional ceramic nanolattices," Science **345**, 1322–1326 (2014).
131. L. A. Shaw, S. Chizari, M. Shusteff, H. Naghsh-Nilchi, D. Di Carlo, and J. B. Hopkins, "Scanning two-photon continuous flow lithography for synthesis of high-resolution 3D microparticles," Opt. Express **26**, 13543–13548 (2018).
132. M. Malinauskas, A. Žukauskas, G. Bičkauskaitė, R. Gadonas, and S. Juodkazis, "Mechanisms of three-dimensional structuring of photopolymers by tightly focussed femtosecond laser pulses," Opt. Express **18**, 10209–10221 (2010).
133. X. Zheng, J. R. Deotte, M. P. Alonso, G. R. Farquar, T. H. Weisgraber, S. Gemberling, H. Lee, N. X. Fang, and C. M. Spadaccini, "Design and optimization of a light-emitting diode projection micro-stereolithography three-dimensional manufacturing system," Rev. Sci. Instrum. **83**, 125001 (2012).
134. M. P. D. Beer, H. L. V. D. Laan, M. A. Cole, R. J. Whelan, M. A. Burns, and T. F. Scott, "Rapid, continuous additive manufacturing by volumetric polymerization inhibition patterning," Sci. Adv. **5**, eaau8723 (2019).
135. A. Ovsianikov, J. Viertl, B. N. Chichkov, M. Oubaha, B. D. Maccraith, I. Sakellari, A. Giakoumaki, D. Gray, M. Vamvakaki, M. Farsari, and C. Fotakis, "Ultra-low shrinkage hybrid photosensitive material for two-photon polymerization microfabrication," ACS Nano **2**, 2257–2262 (2008).

136. T. Buckmann, N. Stenger, M. Kadic, J. Kaschke, A. Frolich, T. Kennerknecht, C. Eberl, M. Thiel, and M. Wegener, "Tailored 3D mechanical metamaterials made by dip-in direct-laser-writing optical lithography," Adv. Mater. **24**, 2710–2714 (2012).
137. R. Batchelor, T. Messer, M. Hippler, M. Wegener, C. Barnerkowollik, and E. Blasco, "Two in one: light as a tool for 3D printing and erasing at the microscale," Adv. Mater. **31**, 1904085 (2019).
138. J. Fischer and M. Wegener, "Three-dimensional direct laser writing inspired by stimulated-emission-depletion microscopy," Opt. Mater. Express **1**, 614–624 (2011).
139. R. Wollhofen, J. Katzmann, C. Hrelescu, J. Jacak, and T. A. Klar, "120 nm resolution and 55 nm structure size in STED-lithography," Opt. Express **21**, 10831–10840 (2013).
140. J. Fischer, J. B. Mueller, A. S. Quick, J. Kaschke, C. Barnerkowollik, and M. Wegener, "Exploring the mechanisms in STED-enhanced direct laser writing," Adv. Opt. Mater. **3**, 221–232 (2015).
141. J. Kaschke and M. Wegener, "Gold triple-helix mid-infrared metamaterial by STED-inspired laser lithography," Opt. Lett. **40**, 3986–3989 (2015).
142. J. Fischer, G. V. Freymann, and M. Wegener, "The materials challenge in diffraction-unlimited direct-laser-writing optical lithography," Adv. Mater. **22**, 3578–3582 (2010).
143. P. Muller, R. Muller, L. Hammer, C. Barnerkowollik, M. Wegener, and E. Blasco, "STED-inspired laser lithography based on photoswitchable spirothiopyran moieties," Chem. Mater. **31**, 1966–1972 (2019).
144. H. Ni, G. Yuan, L. Sun, N. Chang, D. Zhang, R. Chen, L. Jiang, H. Chen, Z. Gu, and X. Zhao, "Large-scale high-numerical-aperture super-oscillatory lens fabricated by direct laser writing lithography," RSC Adv. **8**, 20117–20123 (2018).
145. L. Jonušauskas, D. Gailevičius, S. Rekštytė, T. Baldacchini, S. Juodkazis, and M. Malinauskas, "Mesoscale laser 3D printing," Opt. Express **27**, 15205–15221 (2019).
146. L. Jonušauskas, T. Baravykas, D. Andrijec, T. Gadišauskas, and V. Purlys, "Stitchless support-free 3D printing of free-form micromechanical structures with feature size on-demand," Sci. Rep. **9**, 17533 (2019).
147. S. K. Saha, C. Divin, J. Cuadra, and R. M. Panas, "Effect of proximity of features on the damage threshold during submicron additive manufacturing via two-photon polymerization," J. Micro Nano-Manuf. **5**, 031002 (2017).
148. D. Yang, L. Liu, Q. Gong, and Y. Li, "Rapid two-photon polymerization of an arbitrary 3D microstructure with 3D focal field engineering," Macromol. Rapid Commun. **40**, 1900041 (2019).
149. M. J. Beauchamp, H. Gong, A. T. Woolley, and G. P. Nordin, "3D printed microfluidic features using dose control in X, Y, and Z dimensions," Micromachines **9**, 326 (2018).
150. X. Wan and R. Menon, "Proximity-effect correction for 3D single-photon optical lithography," Appl. Opt. **55**, A1–A7 (2016).
151. T. Stichel, B. Hecht, S. Steenhusen, R. Houbertz, and G. Sextl, "Two-photon polymerization setup enables experimental mapping and correction of spherical aberrations for improved macroscopic structure fabrication," Opt. Lett. **41**, 4269–4272 (2016).
152. Y. Fujishiro, T. Furukawa, and S. Maruo, "Simple autofocusing method by image processing using transmission images for large-scale two-photon lithography," Opt. Express **28**, 12342–12351 (2020).
153. L. Bauch, S. Gruss, A. Teipel, and H. Froehlich, "Method for detecting positioning errors of circuit patterns during the transfer by means of a mask into layers of a substrate of a semiconductor wafer," U.S. patent application 20050068515 (March 31, 2005).